Determining Stability of Organic Solvent Nanofiltration Membranes by Cross-flow Aging

Ze-Xian Low[1,2,3*], *Junjie Shen*[1,2*]

[1] Department of Chemical Engineering, University of Bath, Bath BA2 7AY, UK

[2] Centre for Advanced Separations Engineering, University of Bath, Bath BA2 7AY, UK

[3] Department of Chemical Engineering, Monash University, Clayton VIC 3800, Australia

*Corresponding authors

Email address: nicholas.low@monash.edu (ZX Low), J.Shen@bath.ac.uk (J Shen)

Telephone: +44 (0) 1225 383584

Postal address: Department of Chemical Engineering, University of Bath, Claverton Down, Bath, BA2 7AY, UK

Abstract

Organic solvent nanofiltration (OSN) membranes suffer from performance loss over an extended timescale due to aging. Short-term aging tests often conducted in membrane studies may not be representative of the actual behavior of the OSN membranes when used in organic solvents. There is a need to test the performance of OSN membranes in a way that is more relevant to industrial OSN applications. In this work, we conducted a series of aging tests in two different modes to determine the behavior of 4 commercial OSN membranes (Duramem 200, Puramem 280, GMT-oNF2, and SolSep BV010206) in polar and non-polar organic solvents (i.e., methanol, acetonitrile, and toluene). Firstly, we conducted a 30-day static aging experiment to investigate the stability of four commercial OSN membranes when soaked in the selected solvents. Secondly, we proposed a three-week cross-flow aging protocol with a staged temperature raise to determine the long-term stability of the membranes in real-world scenarios. The operating temperature was controlled between 25 °C and 40 °C in the three-week aging test. The results showed that acetonitrile had the most significant effect on the membranes, and the permeances of the membranes were dependent on the solubility parameters of the polymer and the solvent when the membranes are soaked in the solvents in static operation. The polyimide-based membranes exhibited a noticeable sign of aging with increasing temperature, which could be due to compaction and densification. Our results suggested that the new cross-flow aging protocol can facilitate the rapid screening of OSN membranes for industrial use.

Keywords: stability, membrane aging, organic solvent nanofiltration (OSN), solvent resistant nanofiltration (SRNF), cross-flow

1. Introduction

Separations of solutes in organic solvents play a crucial role in pharmaceutical and chemical processes [1]. Conventional separation techniques in industrial processes include distillation, adsorption, and chromatography that typically involve the use of fresh solvent, large footprint, and high energy cost [2]. Organic solvent nanofiltration (OSN) is an emerging separation process that not only can provide the necessary molecular discrimination without the need for fresh solvent or additives, but also does not involve any phase transition, eliminating thermal damage to high-value products and the need for a high amount of energy (accounting for 80% of the energy associated with separation techniques such as distillation and evaporation that rely on phase change) [1, 3, 4]. The technique has been widely investigated for extensive ranges of industrial processes, including solute enrichment [5, 6], solvent recovery [7, 8], solvent exchange [9, 10], and purification (impurity removal [2, 11], OSN-assisted chemical synthesis [12, 13], OSN-assisted crystallization [14, 15] and catalytic processes [16-19] that otherwise can be challenging for conventional separation techniques.

Unlike nanofiltration, where the separation of solute occurs in aqueous solution, OSN is performed under harsher and more corrosive environments typically required for pharmaceutical and chemical processes [1, 3]. The solvent and pH resistance of the membrane until today remains as one of the main challenges for implementing OSN in relevant processes [20]. The screening of new polymers in search of solvent and pH stable membrane for OSN is often performed by a traditional approach such as soaking the membrane in the solvent of interest for a fixed time. The membrane is subsequently investigated for its stability in the solvent by its solubility, degree of swelling, and solvent permeance measurement. However, most studies measured solvent permeance and solute rejection of OSN membranes in a short duration (typically a few hours) [21]. The performance measured within a short period may not

represent the long-term performance of the membrane [21]. Longer aging studies (e.g. [20-24]) are necessary to determine the actual performance of newly developed membranes.

The long-term stability of OSN membranes is a crucial criterion for industrial applications. Generally, OSN membrane may experience a different form of performance loss over time (decline in permeance, solute rejection, or both) due to fouling, compaction, and/or aging of the membrane [25]. Aging refers to the rearrangement of polymer chains in the amorphous polymer membrane from a non-equilibrium state towards an ever-unachievable equilibrium state [26-28]. The aging phenomenon is often associated with the non-equilibrium state of the glassy polymer when its film is processed to below its glass transitional temperature [26-28]. Most OSN membranes in the market are glassy polymers, which age over time, as evident from their permeance decline during membrane operation [24, 29, 30]. To determine the suitability of a membrane for a separation process on an industrial scale, the membrane often undergoes comprehensive stress test protocols, where the membrane module is subjected to alternating pressure and cleaning cycle using the desired feed stream. Such a stress test is seldom performed on a newly developed membrane in academic research (see **Table S1** for the differences in membrane performance characterization protocol in academia and industry).

In academic studies, OSN membrane performance is usually studied using membrane coupons in ambient conditions, bench-scale, and shorter time (typically a few hours) [31]. On the contrary, the industrial OSN membrane test involves testing the spiral-wound membrane module in 'real-world' condition, pilot to industrial scale, and extended timescale (several months to years) [24]. Often, despite promising membrane performance obtained in academic studies, few membranes can make their way to industrial use. Le Phuong *et al.* identified a gap between academic results and industrial requirements for OSN, which is due to the paucity of information on the long-term stability of membranes and the limited information on industrially relevant filtration [31].

In this work, we propose an OSN membrane aging protocol that is more practicable in terms of time scale. A three-week membrane cross-flow aging with staged temperature raise is proposed to determine the performance of an OSN membrane in different solvents. To demonstrate this, four commercial membranes with comparable solute rejection rate and solvent stability from different OSN membrane manufacturers were investigated (Evonik, UK; SolSep BV, The Netherlands; Borsig Membrane Technology GmbH, Germany). Three different types of industrial relevant solvents were used in this work— methanol (polar protic), acetonitrile (polar aprotic), and toluene (non-polar). The membranes were tested in cross-flow mode and characterized by their cross-flow performance, dye rejection, surface morphology, and contact angle before and after aging. The new membrane characterization protocol may better represent the actual performance and stability of the OSN membranes relevant to membrane industry application and facilitate the screening of new polymer membrane for industrial application.

2. Materials and Methods

2.1. Membranes

Four OSN membranes were used in the experiment: Duramem 200 is an OSN membrane based on a modified polyimide manufactured by Evonik (UK); Puramem 280 is based on polyimide manufactured by Evonik (UK); GMT-oNF2 is a silicone polymer-based composite manufactured by BORSIG Membrane Technology GmbH (Germany) that has an active layer of polydimethylsiloxane (PDMS) on polyacrylonitrile (PAN) support [32]; SolSep BV 010206 is based on polyimide manufactured by SolSep BV (The Netherlands). All four OSN membranes were reported to be generally stable in alcohols, aromatic and aliphatic hydrocarbons, ketones, and ethers. Specifications of each commercial membrane are summarized in **Table 1**.

Table 1. Specifications of selected commercial membranes from the manufacturers.

Membrane	Type	Permeance (L $m^{-2} h^{-1} bar^{-1}$)	MWCO (g mol^{-1}) / rejection (%)	Max T (°C)	Max P (bar)
Duramem 200	modified polyimide (P84)	-	200 (polystyrene in acetone)	50	60
Puramem 280	polyimide	0.6 (toluene)	280 (polystyrene in toluene)	50	60
GMT-oNF2	silicone composite	2 (toluene)	507 / 98% (hexatriacontane)	60	35
SolSep BV 010206	polyimide	1 (acetone)	300 / 95% (fatty acid in acetone)	120	20

2.2. Solvents

Methanol and acetonitrile, HPLC grade, were purchased from Fisher Scientific, UK. Toluene, anhydrous, was purchased from Sigma-Aldrich, UK. The physicochemical properties of the solvents are summarized in **Table 2**. Methylene Blue hydrate (MB) and Sudan Blue II (SB) were purchased from Sigma-Aldrich, UK.

Table 2. Physical and solvent properties [33].

Solvent	**Physical properties**						**Solvent properties**			
	Chemical Formula	**Molecular weight (g mol^{-1})**	**Density (g mL^{-1})**	**Boiling Point (°C)**	**Surface tension (mN m^{-1})**	**Viscosity (mPa^{-1} s^{-1})**	**Dielectric constant (As Vm^{-1})**	**Dipole moment (D)**	**Polarity**	**Hansen solubility parameter ($MPa^{0.5}$) [34]**
Methanol	CH_3-OH	32	0.791	64.0	22.6	0.60	32.6	1.7	76.2	29.6
Acetonitrile	CH_3-C≡N	41	0.786	81.6	29.1	0.38	37.5	3.2	46	24.4
Toluene	C_6H_5-CH_3	92	0.867	110.6	28.5	0.59	2.38	0.4	9.9	18.2

2.3. Characterization

Membrane surface and cross-sectional images were obtained using a scanning electron microscope (SEM; JEOL SEM6480LV, Japan). The membrane was fractured in liquid nitrogen to retain the membrane structure for cross-section imaging. The membrane samples were dried under vacuum at room temperature and sputter-coating with Au before imaging. The water contact angles of the membranes were measured using a contact angle goniometer by the sessile drop technique (OCA15, Dataphysics, Germany). Images were taken at 1 s intervals for 10 s. An average of five measurements was reported for each sample. Three samples were collected for each aging experiment in the same solvent, and the standard deviation is determined from all the contact angle measurements for each aging experiment. The morphologies of the samples were examined using an atomic force microscope (AFM; Nanosurf EasyScan 2 Flex, Switzerland). The samples were taped onto a glass slide and scanned in tapping mode (scan size of 1 × 1 μm and 5 × 5 μm, time/line of 1 s, samples/line of 256) with a monolithic silicon AFM probe (Tap190Al-G, BudgetSensors, Bulgaria) for the different projected area. The probe had a spring constant of 48 N m^{-1}, the resonant frequency of 190 kHz, and a nominal tip radius of < 10 nm.

2.4. Static aging

The commercial membranes were cut to coupons of 25 mm in diameter and weighed. The weighed samples were then put in methanol, acetonitrile, and toluene in separate vials for 30 days at room temperature. After 30 days, the coupons were taken out and carefully wiped with filter paper to remove the solvent on the membrane surface. The swelling coefficient was determined by measuring the weight increase relative to the dry weight after swelling. The swelling coefficient, Q is defined by [35]

$$Q = \frac{m - m_0}{m_0} \times \frac{1}{\rho_s}$$

where m is the weight of the swollen sample, m_0 is the weight of the dried sample, and ρ_s is the density of the solvent. Images of the sample surfaces were taken after the measurement.

2.5. Cross-flow aging

A schematic diagram of the cross-flow aging is shown in **Figure 1(a)**. The setup consists of a diaphragm metering pump (Hydracell with PTFE diaphragm and O-rings), four flat sheet circular membrane cells, pressure gauge and thermocouple, oil bath, pressure relief valve, and 3-way valves. The effective membrane area of the circular membrane coupon was 1.4×10^{-3} m^2. The membrane cells have a space channel of 5 mm between the membrane and the wall of which the feed is passed. The permeate was collected as needed or otherwise circulated back into the feed tank.

The three-week cross-flow aging experiment was performed on Duramem 200, Puramem 280, GMT-oNF2, and SolSep BV 010206 using different organic solvents as the feed. The operating conditions for cross-flow aging were chosen based on the typical operating conditions of each membrane provided by its manufacturer (**Table 1**) and the boiling point of each solvent (**Table 2**). The fresh membranes were pretreated using fresh solvent at 30 bar for 2 h to remove pore preservatives and was then compacted for 24 h at the same pressure. Afterwards, the feed stream was maintained at 30 bar and 500 mL min^{-1} throughout the experiment, and the permeance was collected and measured periodically.

The temperature of the cross-flow aging was controlled at three different cycles. The measurement was performed at 25 °C for the 1st week before raising to 30 °C in the 2nd week and subsequently 35 or 40 °C in the 3rd week, depending on the solvent used (**Figure 1(b)**). The actual temperature of the feed passing through the membrane cells was measured by thermocouples at locations before the feed entering the first membrane cell and right after the feed exiting the last cell. The average temperature of the feed before and after passing all four

membrane cells were reported. All measurements were performed in an enclosed chamber in a walk-in fume cupboard to ensure safety compliance.

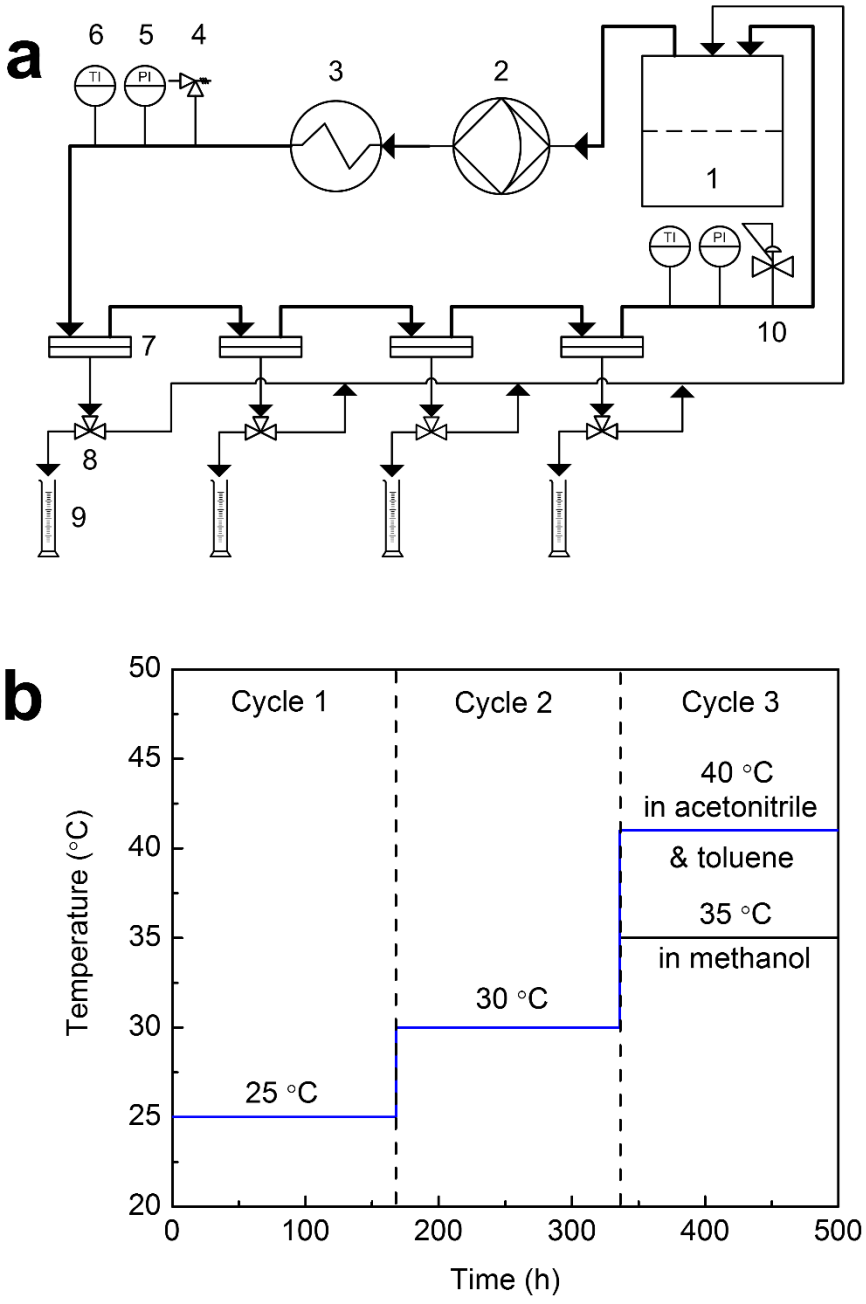

Figure 1. (a) Schematic diagram of the 4-cell cross-flow rig used in this study. Legend: 1: Solvent tank, 2: pump, 3: oil bath, 4: pressure relief valve, 5: pressure gauge, 6: thermocouple, 7: flat-sheet membrane cell, 8: three-way valve, 9: measuring cylinder, 10: backpressure regulator and (b) schematic representation of the temperature cycles in this study.

2.6. Rejection of dyes

At the end of each cross-flow aging protocol, the dye rejection of the membranes was tested. MB (M_w of 320 Da) was used as the molecule probe in methanol and acetonitrile, while SB (M_w of 350 Da) was used in toluene. The dye rejection test was performed only for compatible solvents of the membranes with measurable permeance. The dye rejection was calculated using the classical rejection coefficient:

$$R(\%) = \left[1 - \frac{C_p}{C_0}\right] \times 100$$

where C_0 is the initial concentration of the dye in the feed solution and C_p is the dye concentration in the permeate.

The concentrations of MB and SB were determined using a UV spectrophotometer (Cary 100 UV-Vis, Agilent, USA) at a wavelength of 290 and 285 nm, respectively. Calibration curves of absorbance of the dye solutions of known concentrations were prepared to determine the concentration of the dye in the permeate (**Figure S1**).

3. Results and Discussion

3.1. Static aging

3.1.1. Membrane morphology

A static aging experiment of 30 days was performed to determine the stability of Duramem 200, Puramem 280, SolSep BV 010206, and GMT-oNF2 in the selected solvents. The top-down images of the membranes were captured on the 30th day of the static aging (**Figure S2**). All membranes did not show any noticeable difference in the membrane surface in different organic solvents, suggesting that the membranes were sufficiently stable throughout the static aging. Darkening of membranes such as in Duramem 200 and SolSep BV010206 was observed, but such darkening over time was normal as expected, as stated in

the membrane datasheet. The colour change was likely accelerated by the solvents. Duramem 200 and Puramem 280 showed some signs of curling in the air after they were gently wiped to remove the solvent on their surfaces. This is due to the removal of pore preservatives in the asymmetrical polymer structure of both membranes during pretreatment. The evaporation of the solvent in the polymer matrix and the rigid polyester support layer at different rates cause the membrane to curl.

AFM was performed on the samples before and after the static aging to determine the changes to the surface roughness caused by the solvents (**Figure 2**). Surface roughness (S_a) data derived from AFM analyses give quantitative insights into the surface morphology of the commercial membranes. SolSep BV010206 showed significantly higher S_a values compared to the other three membranes. In the imaging size of 5 micron × 5 micron, both Duramem 200 and Puramem 280 show increased roughness after 30 days in the solvents, while Solsep BV010206 and GMT-oNF2 show reduced roughness. The initial lower roughness value showed by both the pristine membranes of Duramem 200 and Puramem 280 may be due to the spreading of a layer of pore preservatives. Thus, the washing out of pore preservatives during the static aging may cause the roughness to increase. In the imaging size of 1 micron × 1 micron, a significant increase in roughness was observed for GMT-oNF2 while the remaining membranes experienced decreased roughness (**Figure S3, S4, and Table S2**). This likely might be due to the nature of the polymer used (PDMS vs polyimide). Even though all membranes tested in this study remained stable after the static aging, changes to the surface property in the microscopic scale suggest that the actual membrane performance of these membranes may be influenced by their exposure to different solvents.

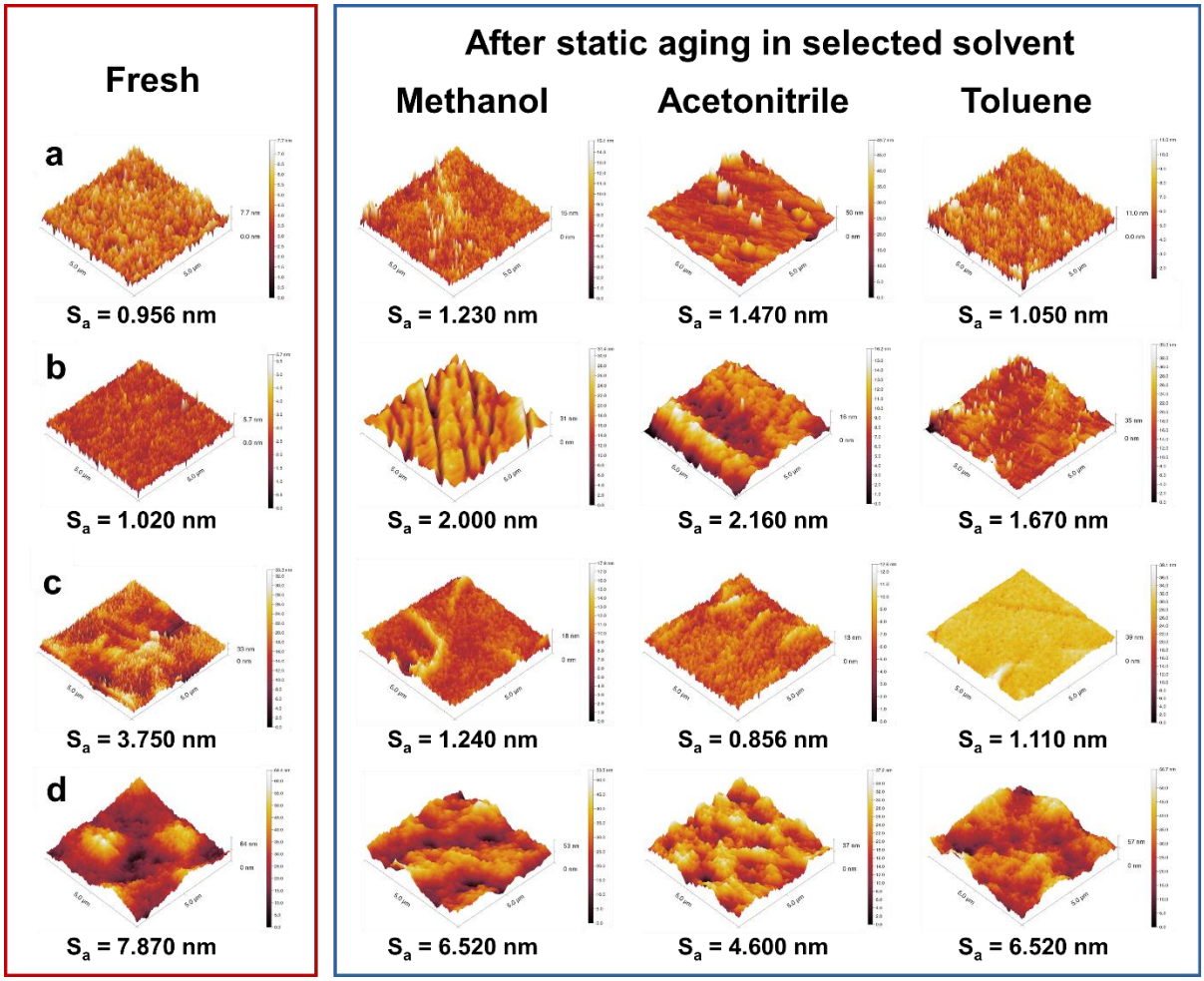

Figure 2. AFM images and surface roughness (S_a) values of (a) Duramem 200, (b) Puramem 280, (c) GMT-oNF2, and (d) Solsep BV010206 before and after static aging for 30 days (scale: 5 μm × 5 μm).

3.1.2. Membrane hydrophilicity

The hydrophilicity of the OSN membranes was investigated using water contact angle goniometry. As expected, GMT-oNF2 shows the contact angles much higher than the other three membranes, consistently above 105° (**Table 3**). The contact angle is comparable to results obtained for PDMS surfaces in the other work (108–115°) [36, 37]. The other three OSN membranes generally show a typical contact angle of polyimide of 75–81° (after the static aging) [38, 39]. The contact angle and wetting behavior of a solid sample is influenced by its surface geometry and chemical properties [40].

Given that we lack the information on the actual composition of the commercial OSN membranes in this work and unable to conduct any work that could relate to the chemical structure of the membrane, we are unable to provide information on the changes to the chemical properties. The results from the contact angle, on the other hand, are consistent with the trends observed in the changes to the surface roughness, S_a. It appears that acetonitrile has the most significant effect on the OSN membranes and that OSN membranes were likely to be least stable in acetonitrile. A similar trend was reported in a previous study [41]. According to Wenzel's equation [42], the higher contact angle exhibited by the membranes with a hydrophilic surface (Duramem 200, Puramem 280, and Solsep BV010206) suggests that the membranes have a smoother surface after the static aging. The membrane with a hydrophobic surface such as GMT-oNF2 showing a higher contact angle suggests the roughening of the membrane surface after the static aging. The results are consistent with results obtained from AFM.

Table 3. Water contact angle (º) of Duramem 200, Puramem 280, GMT-oNF2, and SolSep BV010206 before and after static aging for 30 days.

Sample	**Fresh**	**Solvent**		
		Methanol	**Acetonitrile**	**Toluene**
Duramem 200	51.76 ± 1.26	71.56 ± 4.80	87.44 ± 2.09	60.52 ± 5.86
Puramem 280	70.18 ± 2.10	72.06 ± 5.08	91.70 ± 5.45	86.02 ± 3.50
GMT-oNF2	107.28 ± 1.73	108.86 ± 1.07	105.96 ± 1.64	110.36 ± 0.61
Solsep BV010206	68.02 ± 2.59	85.36 ± 1.86	78.10 ± 2.53	86.04 ± 1.91

3.1.3. Membrane swelling

The swelling coefficient of the polymer membrane can be used as an indicator of the interaction with the solvent. The swelling coefficients of the four commercial OSN membranes were plotted against the Hansen solubility parameters of the solvents (**Figure 3a**). Hansen

solubility parameters are typically used to account for dispersion forces, polar forces, and hydrogen bonds between molecules [34]. A polymeric membrane is likely to swell in a solvent if they have similar Hansen solubility parameters [43]. The Hansen solubility parameters (25 °C) of the solvents are: 29.6 $MPa^{0.5}$ (methanol), 24.4 $MPa^{0.5}$ (acetonitrile), and 18.2 $MPa^{0.5}$ (toluene), respectively [44]. However, the Hansen solubility parameters of the commercial OSN membranes are not known because chemical compositions of these membranes deem to be proprietary and confidential. As a result, solubility parameters of several commercial polymers were used as rough estimates (dashed lines in **Figure 3**). These polymers include one PDMS [45-47] and four polyimides, namely Ultem 1000 (General Electric, notation: UT) [48, 49], Matrimid 5218 (Huntsman, notation: MAT) [48, 50], P84 (HP Polymer, notation: P84) [48, 51], and HT P84 (HP Polymer, notation: HT) [50, 51]. It can be seen that the solubility parameters of commercial polyimides (UT, MAT, P84, and HT) vary widely, depending on the diamine and dianhydride of the polyimide [52]. The chemical structures of the polyimides are available in **Figure S5**.

Duramem 200 shows an increasing swelling coefficient from non-polar to polar solvent, suggesting that the membrane may perform better in polar solvents than non-polar solvent. Puramem 280, on the other hand, shows a significantly higher swelling coefficient than Duramem 200 in all three solvents. Both GMT-oNF2 and SolSep BV 010206 show significantly higher swelling coefficients than the former two membranes. SolSep BV 010206, which is also based on polyimide, shows a similar swelling coefficient regardless of the solvents used. The difference in the swelling coefficient of SolSep BV 010206 compared to other polyimide membranes used in this study can potentially be attributed to the type of polyimide, degree of crosslinking, and membrane preparation method used. GMT-oNF2, which is a silicon composite membrane, also shows higher swelling coefficients than most polyimide-based membranes. The higher swelling can arise from the silicon component of the

membrane, which tends to swell, just like most rubbery materials [37]. The solvent permeance of the membranes will be further discussed in the next section.

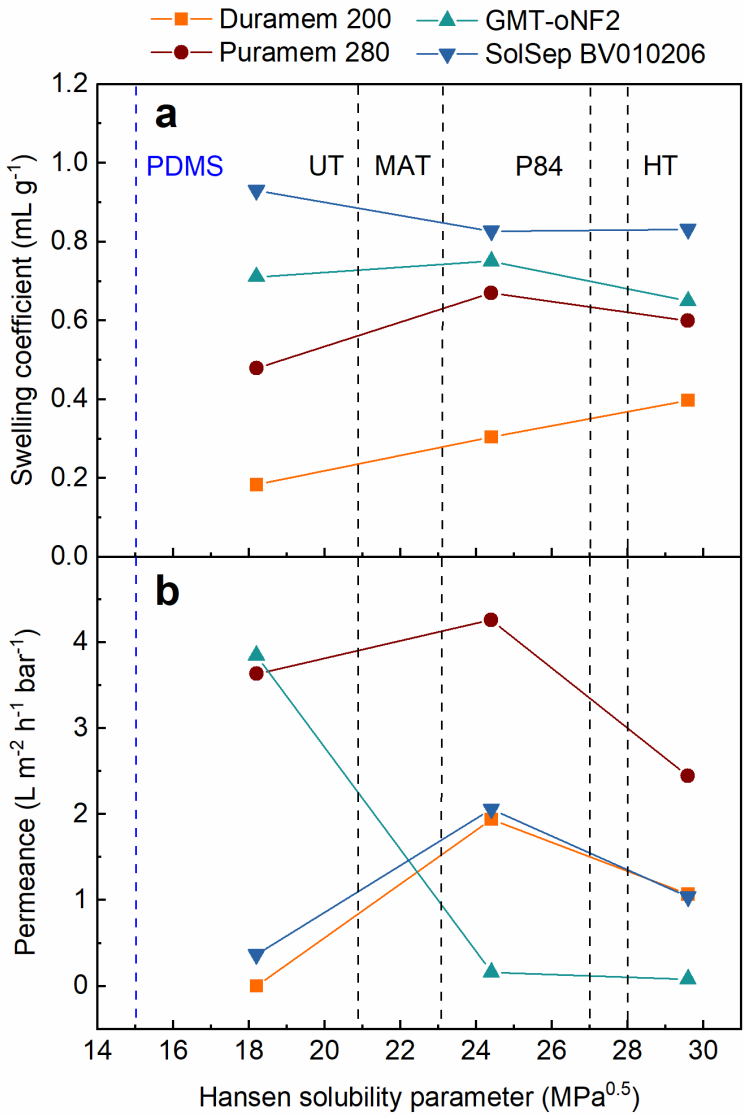

Figure 3. (a) Swelling coefficient, Q and (b) solvent permeance of Duramem 200, Puramem 280, GMT-oNF2, and SolSep BV010206 after static aging for 30 days as a function of Hansen solubility parameter of solvent (methanol: 29.6 $MPa^{0.5}$; acetonitrile: 24.4 $MPa^{0.5}$; and toluene: 18.2 $MPa^{0.5}$).

3.1.4. Solvent permeance

The solvent permeance was obtained after pretreatment of 2 h and pre-compaction of 24 h in the cross-flow mode. The permeances of the four commercial OSN membranes were

plotted against the solubility parameter in **Figure 3b**. Duramem 200 is compatible with a polar solvent (such as methanol and acetonitrile), while GMT-oNF2 is compatible with a non-polar solvent such as toluene. Puramem 280 and SolSep BV010206 show permeances of all solvents used in this study, with a preference for polar solvents. The finding in this work is consistent with that of [53, 54], where Puramem 280 shows higher permeance for toluene compared to methanol [53] and where similar methanol permeance was obtained [54]. The commercial membrane may not necessarily be suitable for the solvent in which it is stable, as shown by the different preference of Duramem 200 and GMT-oNF2 to polar and non-polar solvents, respectively. GMT-oNF2, which is a PDMS membrane with PAN support, show relatively low permeance for methanol and acetonitrile and much higher toluene permeance of 3.8 L m^{-2} h^{-1} bar^{-1}. A similar performance of GMT-oNF2 was also observed for methanol and toluene in the other work [32].

The permeance of the membranes was reported to be dependent on the solubility parameter [32, 43, 55, 56]. The closer the solvent solubility parameter of the solvent to that of the membrane, the higher the measured permeance. Therefore, the interactions between the membrane and the solvents can be predicted from the solubility parameter of the membrane and the solvents. Such representation can be more meaningful than swelling measurements when comparing the stability of different OSN membranes, which differ in polymer, structure, thickness, and backing layer. It was also reported that other important parameters that influence the permeance are solvent polarity and molecular size, but the influences are less pronounced [21, 57]. GMT-oNF2 shows permeances that are consistent with those observed for PDMS membranes since PDMS has the closest solubility parameter to toluene, followed by acetonitrile and methanol [32]. All other polyimide type OSN membranes showed the same trend with the highest acetonitrile permeance. It appeared that Puramem 280 might have a solubility parameter more like UT and MAT, while Duramem 200 and SolSep BV010206 may

have solubility parameters more like P84 and HT. Typical bell-shaped curves were observed for polyimide-based membranes such as Duramem 200, Puramem 280 and SolSep BV010206. However, the bell-shaped curve cannot be obtained for a PDMS membrane since there is no solubility parameter significantly lower than that of PDMS.

Generally, the commercial membranes based on polyimide show the highest permeance in acetonitrile compared to other organic solvents using the same membrane. The permeance results are consistent with the morphology and hydrophilicity results, where the most substantial changes to roughness and water contact angle were obtained in acetonitrile. There were only a few applications of commercial OSN membranes available in the market for solvents such as acetonitrile [41, 58-61]. Only very recently, some newly developed OSN membranes based on polybenzimidazole (PBI) [20, 62-66] and polyelectrolyte [62] were tested in acetonitrile.

3.2. Cross-flow aging

While a static aging experiment can provide some useful information on the membrane stability, a cross-flow test that resembles more closely to the actual separation process can provide a better insight into the long-term stability of the OSN membranes in these solvents. Unlike static aging, the solvent was circulated, and the membranes were pressurized on the feed side. The operating conditions, such as pressure, cross-flow velocity, and temperature, can be varied. The experiment was performed on a membrane coupon to understand the behaviour of the polymer film. Under such conditions, the changes to the membrane properties (physically or chemically) can be quantitatively measured *in situ* by measuring the solvent permeance of the membranes tested.

3.2.1. Membrane morphology

After the three-week cross-flow aging, all membranes (including fresh and unused membranes) were fractured under liquid nitrogen for cross-section analysis. The backing layers

of the membranes were removed when possible to allow fracture of membranes under liquid nitrogen. Evidence of membrane compaction is prominent in SEM images of the membrane cross-section (**Figure 4**). Under membrane operation at 30 bar over three weeks, all membranes show significantly thinner cross-section. Generally, no clear sign of the aging effect is observed on the polymer structure in all the membranes except for SolSep BV010206. SolSep BV010206 has asymmetrical finger-like structures that extend to macrovoids supported on a thick backing layer. After the cross-flow aging, the same structure of the substrate is no longer observed in SolSep BV010206 owing to the significant compaction and aging of the membrane. SEM indicates that the membranes are sufficiently robust in the condition tested, which is consistent with the results obtained from the cross-flow test, where no drastic changes to the solvent permeance throughout the three-week aging protocol in methanol, acetonitrile, and toluene.

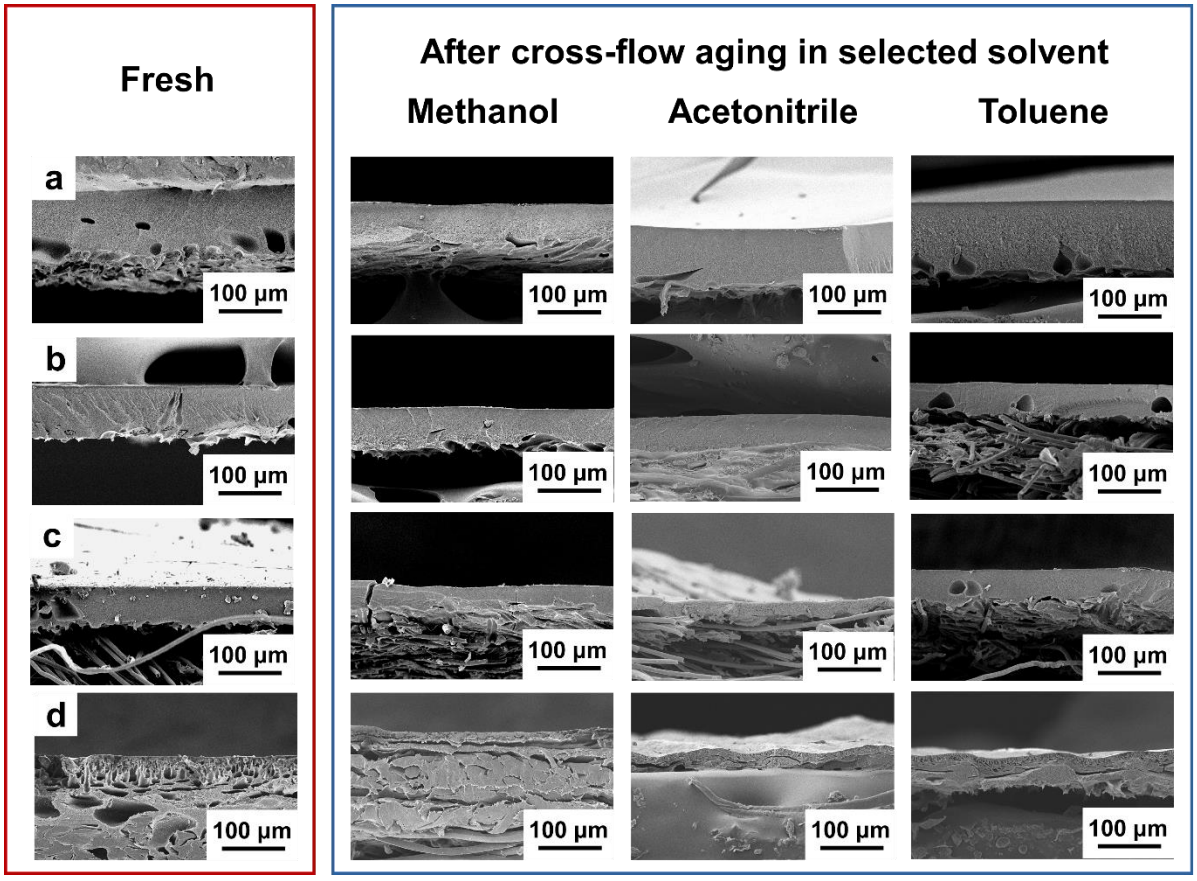

Figure 4. SEM images of (a) Duramem 200, (b) Puramem 280, (c) GMT-oNF2 and (d) SolSep BV010206 before and after the three-week cross-flow aging.

3.2.2. Methanol permeance

Figure 5a and d show the methanol permeance and normalized methanol permeance for the four OSN membranes under investigation. Previous reports have shown that a more extended period of pre-compaction (about three days) is needed before stable permeance can be achieved [21]. The pre-compaction time, in reality, depends on not only the membrane but also the testing condition. We would expect a lower compaction rate (and degree of compaction) at lower transmembrane pressure. Generally, all membranes show decreasing permeance over time, with increased permeance when the temperature is raised. A significant decrease to permeance was observed for Puramem 280 in the first week, which stabilized to ~2.5 L m^{-2} h^{-1} bar^{-1} as the highest methanol permeance among the four membranes tested. The decrease can be ascribed to the compaction of the film, whereby the membrane requires a longer time to stabilize (possibly due to less or no crosslinking of Puramem 280).

When the temperature is raised to 30°C and 35°C, Puramem 280 exhibits an initial increase in permeance, which gradually decreases with time. It appears that the more rapid penetration of solvents through the membrane (due to the decrease in solvent viscosity [67] or intrapore viscosity [68]) causes a change to the membrane structure and the membrane required more time to arrive at a more stable state. The rise in temperature may also increase the polymer chain mobility [69, 70] or affect the sorption/desorption of solvent [68] or solute [71] in pores leading to a similar outcome. These temperature effects on membrane performance have also been observed in other aqueous solutions [72] and organic solutions [73]. Interestingly, the solvent permeance also decreases with time after the temperature was raised to reach a new steady-state close to 2.5 L m^{-2} h^{-1} bar^{-1} but at a higher temperature. This indicates that the membrane has aged.

The deterioration in membrane performance can be due to various factors, including physical aging, chemical aging (degradation or structural changes to polymer chains),

membrane compaction, and fouling. Our results indicate that the physical aging of membrane could have been accelerated under the combined effect of temperature and solvent. Here we also ruled out that the decrease permeance was due to compaction or fouling. Membrane compaction is often correlated to the transmembrane pressure whereby higher pressure leads to a higher loss in membrane porosity (or increased hydraulic resistance) and, therefore, lower permeance [74-77]. On the other hand, the permeation loss caused by fouling is unlikely since pure solvents were used. It is, however, possible for chemical aging to occur. The chemical aging of the membranes was not investigated due to our non-disclosure agreement with the membrane manufacturers. Here we would refer the decrease in permeance (a combination of physical and chemical aging) due to the combined effect of solvent, pressure, and temperature simply as accelerated aging.

Among the four membranes, both Puramem 280 and SolSep BV010206 showed visible signs of accelerated aging, whereby similar steady-state permeances were obtained despite the higher temperature. Duramem 200, a crosslinked polyimide, on the other hand, exhibits more stable permeance, which increases with temperature and stabilizes after a few days. This can be explained by its crosslinked backbone, which resists aging. Any sign of aging that might have occurred in Duramem 200 is offset by the increase in permeance due to the temperature effect, as shown by the higher plateau in Stage II and III of the experiment (stages as indicated by the broken lines). GMT-oNF2, a rubbery polymer, shows no sign of aging during the three-week cross-flow test, with an increase in solvent permeance due to temperature effect.

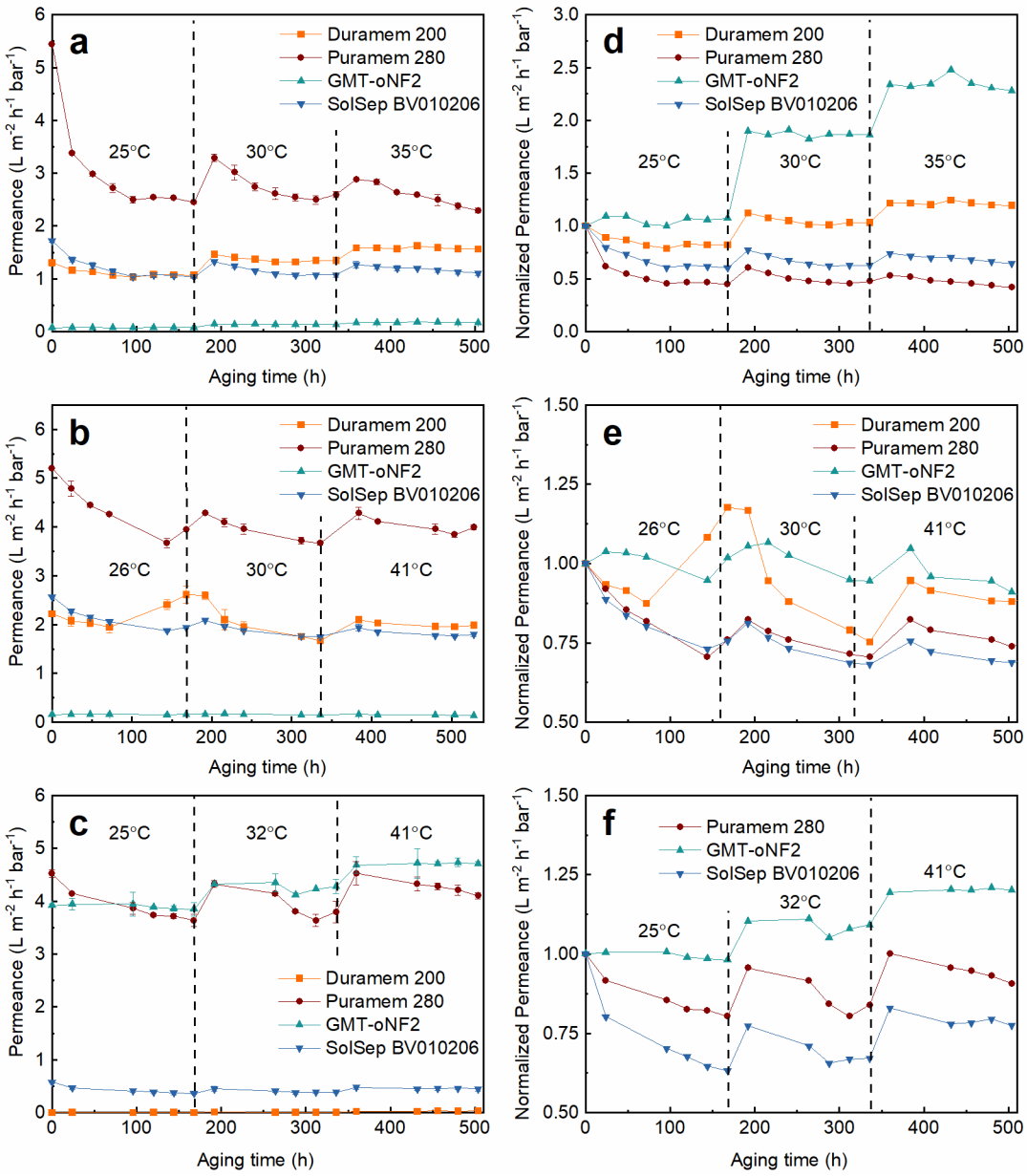

Figure 5. Solvent permeance of Duramem 200, Puramem 280, GMT-oNF2, and SolSep BV 010206 in (a) methanol, (b) acetonitrile, and (c) toluene over three-week aging study. (d–f) Corresponding normalized solvent permeance.

3.2.3. Acetonitrile permeance

We notice the consistent permeance drop in all membranes for two consecutive days over the three-week aging (**Figure S6 and S7**). It was found to be due to the unregulated room temperature at the laboratory over the weekend. The data points of the permeance during the

weekend were removed from the figures (**Figure S6 and S7**) without affecting the trend. **Figure 5b and e** show the acetonitrile permeance and normalized acetonitrile permeance of Duramem 200, Puramem 280, GMT-oNF2, and SolSep BV 010206 over the three-week aging study. Duramem 200 shows an unexpected increase in acetonitrile permeance in the first week, while the other membranes show a similar drop in permeance over time. This could be owing to the lower stability of Duramem 200 in acetonitrile, which causes significant changes to the polymer or membrane structure or incomplete removal of pore preservatives from the membrane matrix until day four. Both AFM (**Figure 2**) and water contact angle analysis (**Table 3**) suggest that the effect of acetonitrile on Duramem 200 and Puramem 280 is the most significant. All glassy polymer membranes (Duramem 200, Puramem 280, and SolSep BV010206) show a clear sign of aging. However, the effect of temperature on the resulting permeance is less significant than that of the methanol system. Negligible acetonitrile permeance is observed for GMT-oNF2.

3.2.4. Toluene permeance

Similarly, the drop in permeance caused by the room temperature drop was omitted from the original plot in the supporting information (**Figure S7**). Generally, the commercial OSN membranes show more stable toluene permeance than in methanol and acetonitrile (**Figure 5c and f**). GMT-oNF2, for instance, shows highly stable toluene permeance that increases with temperature, with no noticeable sign of aging. The permeance stability of GMT-oNF2 could be explained by its rubbery that is in the equilibrium state. The results from the static aging could not reflect the stability of GMT-oNF2 in cross-flow performance. Puramem 280, on the other hand, shows visible signs of accelerated aging with increasing temperature in toluene compared to in methanol and acetonitrile. The result is also consistent with the lower swelling coefficient of Puramem 280 in toluene compared to that in the other two solvents. Duramem 200 shows no permeance to toluene, while SolSep BV010206 shows consistently

low permeance throughout the three cycles. However, SolSep BV010206 also shows a similar sign of aging, as observed in **Figure 5f**.

3.2.5. Rejection of dyes

Membrane solute rejection was characterized by measuring the rejection of MB in methanol and acetonitrile, and SB in toluene using the cross-flow apparatus. **Figure 6** shows the rejection of the dye in different solvents for each membrane (results based on UV adsorption measurement, **Figure S8**). After the three-week aging test, Duramem 200 shows increased dye rejection while the other three membranes show decreasing dye rejection. The increasing solute rejection in Duramem 200 is due to the densification of the cross-linked polyimide, especially near the surface, which results in 'pore' tightening.

On the other hand, a minor drop in solute rejection observed in the other three polymers can be explained by the simultaneous densification and polymer chain rearrangement of non-crosslinked polymer backbones that lead to higher preferences for solute transport over solvent transport. A higher drop in MB in methanol was observed for SolSep BV010206 after three weeks owing to a similar but more significant effect. The result is consistent with that of other aging studies whereby prolonged exposure to solvent at elevated temperature causes a consistent drop in solute rejection [78]. Furthermore, the changes to the solute rejection are highly dependent on the structure and degree of crosslinking of the polymer chains [70, 79, 80].

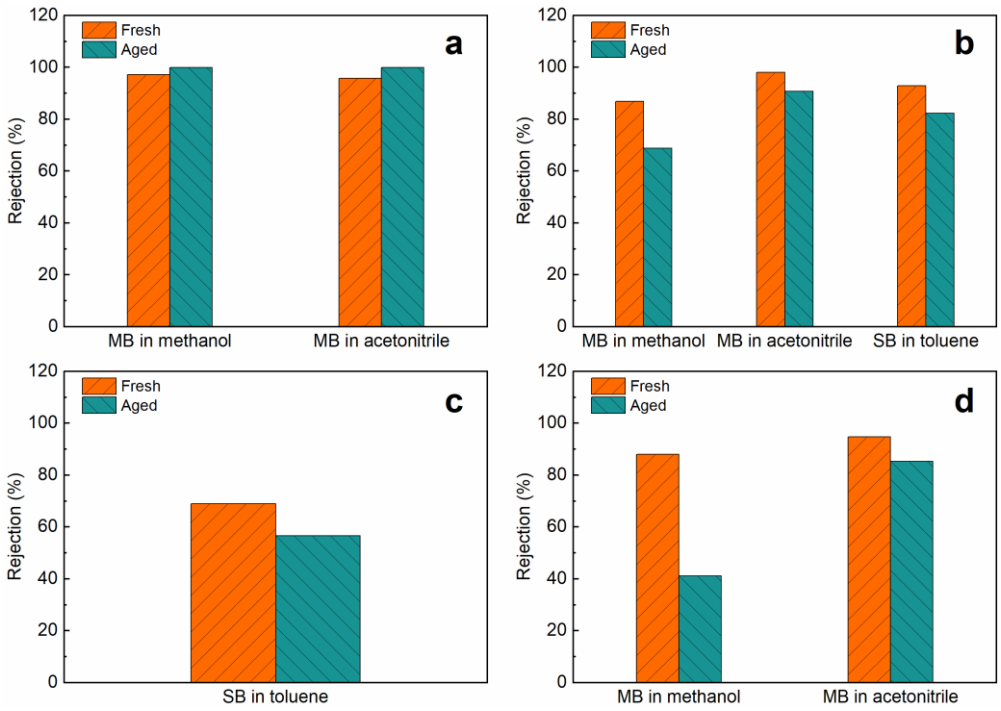

Figure 6. Rejections of MB in methanol, MB in acetonitrile, and SB in toluene of (a) Duramem 200, (b) Puramem 280, (c) GMT-oNF2, and (d) SolSep BV 010206 after the three-week cross-flow aging.

3.3. Aging mechanisms

The effect of aging as probed by the changes to solvent permeance and solute rejection is illustrated in **Figure 7**. **Figure 7a** shows the typical effect of compaction, where exerted pressure reduces the size of the macrovoids within the matrix of the membranes and causes shrinkage to the smaller pores. The membranes were compressed by the exerted pressure, as confirmed by the SEM images (**Figure 4**). Compaction occurs in all membranes when pressure is applied but is often reversible.

Densification, on the other hand, occurs more slowly throughout the matrix of the membranes. An illustration of membrane densification is shown in **Figure 7b**. Reports have shown that densification of the polymer occurs more rapidly near the surface of the membrane due to the higher degree of chain mobility near the membrane surface [81-84]. Unlikely aging of polymer in air, polymer membrane exposed to solvent under operating pressure and

temperature tends to age faster, especially near the surface of the membrane. The additional interaction between the solvent and the membrane increases the mobility of the polymer chain, enabling the polymer chains to reorganize towards a more stable state. Since the membrane made from the non-solvent induced phase separation process has a dense skin layer on top of a highly porous sublayer, the most significant aging effect is expected to be on this layer, where the polymer chains are already in close proximity [81]. The surface changes agreed with the AFM and contact angle measurements. The aging effect can be compared to that of the annealing step following a phase inversion process, but at membrane operating conditions and constant exposure to solvent throughout the membrane use [79, 85-87].

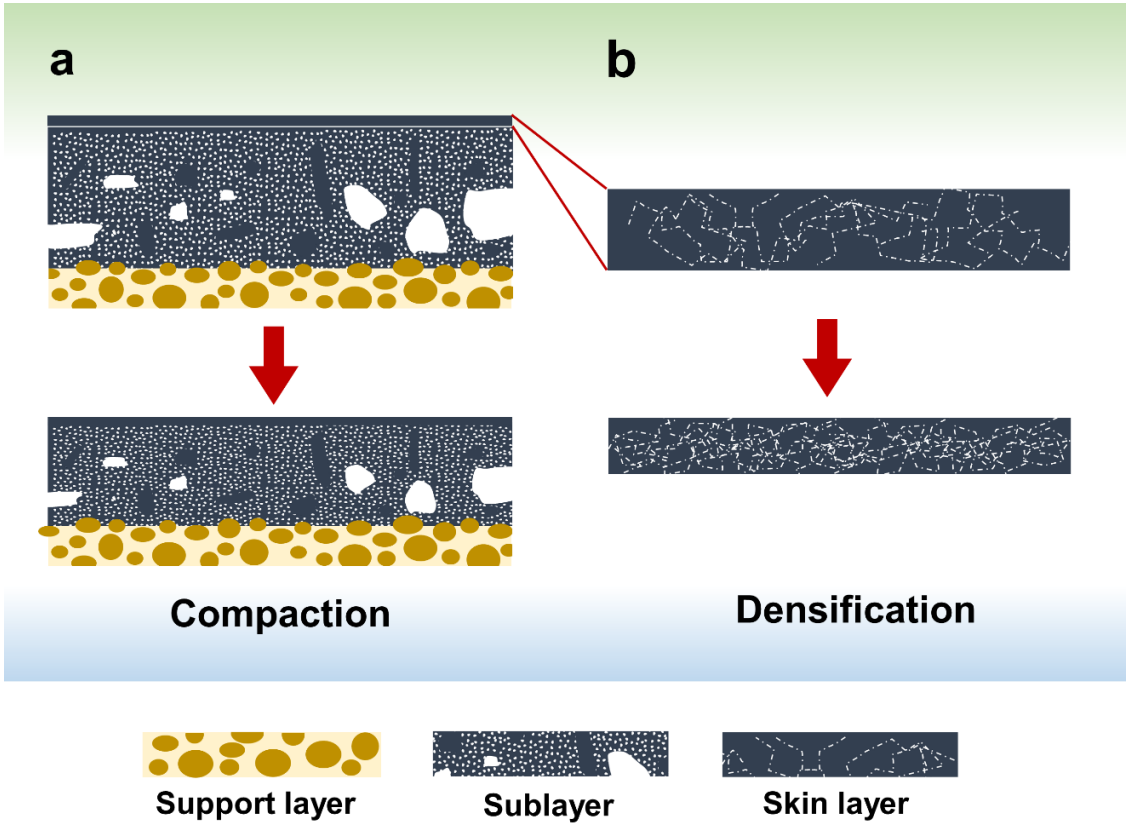

Figure 7. Schematic of (a) compaction and (b) densification of membrane before and after cross-flow aging.

4. Conclusions

We have performed a 30-day static aging test and a three-week cross-flow aging test of four different commercial membranes in both polar and non-polar solvents. The static aging results showed that the OSN membranes were likely to be least stable in acetonitrile, and the permeance and swelling of the membranes were dependent on the solubility parameters of their polymer and the solvent. The cross-flow aging results revealed that the polyimide-based membranes (Duramem 200, Puramem 280, and SolSep BV010206) exhibited a noticeable sign of aging in an organic solvent with increasing operating temperature. GMT-oNF2, with a PDMS active layer, did not suffer from aging in its rubbery state. The aging mechanisms involved compaction and densification. We have also confirmed that the pre-compaction time of the OSN membranes can take more than three days before stable permeance was achieved. This suggests that pure solvent permeance and solute rejection measured in a short period (usually less than one day), as reported in most OSN membrane studies, is inadequate to represent the realistic and stable performance of the membranes. We highly suggest the permeance measurement of newly developed membranes to be performed following this or similar cross-flow aging protocol, allowing sufficient compaction and more rapid aging in the first few weeks over the membrane lifespan. Such a protocol can be a useful tool to accelerate the tedious membrane screening procedures for large-scale manufacturing.

Credit author statement

Ze-Xian Low: Conceptualization, Methodology, Investigation, Data Curation, Writing - Original Draft

Junjie Shen: Investigation, Validation, Visualization, Writing - Review & Editing

Acknowledgment

The work was supported by the Engineering and Physical Sciences Research Council (EPSRC) UK (Programme Grant EP/M01486X/1 (SynFabFun)). The authors wish to acknowledge Dr Kim Wu and Syahira Zulkifli for assisting in sample preparation and preliminary experiments, Prof. Andrew Livingston and Prof. Davide Mattia for the useful discussion, Dr Petra Cameron for the use of AFM, and Dr Wentao Deng and Dr Xinxing Liang for their help in AFM measurement. This manuscript is dedicated to Dr Darrell Alec Patterson (November 14th, 1974 – February 19th, 2017).

References

[1] P. Marchetti, M.F. Jimenez Solomon, G. Szekely, A.G. Livingston, Molecular separation with organic solvent nanofiltration: a critical review, Chemical Reviews, 114 (2014) 10735-10806.

[2] G. Székely, M. Gil, B. Sellergren, W. Heggie, F.C. Ferreira, Environmental and economic analysis for selection and engineering sustainable API degenotoxification processes, Green Chemistry, 15 (2013) 210-225.

[3] P. Vandezande, L.E. Gevers, I.F. Vankelecom, Solvent resistant nanofiltration: separating on a molecular level, Chemical Society Reviews, 37 (2008) 365-405.

[4] R.P. Lively, D.S. Sholl, From water to organics in membrane separations, Nature Materials, 16 (2017) 276-279.

[5] G. Baumgarten, OSN at Evonik, in: 3rd International Conference on Organic Solvent Nanofiltration, 2010.

[6] D. Shi, Y. Kong, J. Yu, Y. Wang, J. Yang, Separation performance of polyimide nanofiltration membranes for concentrating spiramycin extract, Desalination, 191 (2006) 309-317.

[7] J.F. Kim, G. Szekely, M. Schaepertoens, I.B. Valtcheva, M.F. Jimenez-Solomon, A.G. Livingston, In situ solvent recovery by organic solvent nanofiltration, ACS Sustainable Chemistry & Engineering, 2 (2014) 2371-2379.

[8] S. Darvishmanesh, L. Firoozpour, J. Vanneste, P. Luis, J. Degrève, B. Van der Bruggen, Performance of solvent resistant nanofiltration membranes for purification of residual solvent in the pharmaceutical industry: experiments and simulation, Green Chemistry, 13 (2011) 3476-3483.

[9] J.P. Sheth, Y. Qin, K.K. Sirkar, B.C. Baltzis, Nanofiltration-based diafiltration process for solvent exchange in pharmaceutical manufacturing, Journal of Membrane Science, 211 (2003) 251-261.

[10] J. Chun-Te Lin, A.G. Livingston, Nanofiltration membrane cascade for continuous solvent exchange, Chemical Engineering Science, 62 (2007) 2728-2736.

[11] M.B. Martínez, B. Van der Bruggen, Z.R. Negrin, P.L. Alconero, Separation of a high-value pharmaceutical compound from waste ethanol by nanofiltration, Journal of Industrial and Engineering Chemistry, 18 (2012) 1635-1641.

[12] S. So, L.G. Peeva, E.W. Tate, R.J. Leatherbarrow, A.G. Livingston, Membrane enhanced peptide synthesis, Chemical Communications, 46 (2010) 2808-2810.

[13] N.F. Ghazali, D.A. Patterson, A.G. Livingston, Elucidation of the mechanism of chiral selectivity in diastereomeric salt formation using organic solvent nanofiltration, Chemical Communications, (2004) 962-963.

[14] S. Ferguson, F. Ortner, J. Quon, L. Peeva, A. Livingston, B.L. Trout, A.S. Myerson, Use of continuous MSMPR crystallization with integrated nanofiltration membrane recycle for enhanced yield and purity in API crystallization, Crystal Growth & Design, 14 (2013) 617-627.

[15] J. Campbell, L.G. Peeva, A.G. Livingston, Controlling crystallization via organic solvent nanofiltration: The influence of flux on griseofulvin crystallization, Crystal Growth & Design, 14 (2014) 2192-2200.

[16] M. Janssen, C. Müller, D. Vogt, Recent advances in the recycling of homogeneous catalysts using membrane separation, Green Chemistry, 13 (2011) 2247-2257.

[17] A. Livingston, L. Peeva, S. Han, D. Nair, S.S. Luthra, L.S. White, L.M. Freitas Dos Santos, Membrane separation in green chemical processing, Annals of the New York Academy of Sciences, 984 (2003) 123-141.

[18] J. Shen, K. Beale, I. Amura, E.A.C. Emanuelsson, Ligand and solvent selection for enhanced separation of palladium catalysts by organic solvent nanofiltration, Frontiers in Chemistry, 8 (2020).

[19] D. Ormerod, N. Lefevre, M. Dorbec, I. Eyskens, P. Vloemans, K. Duyssens, V. Diez de la Torre, N. Kaval, E. Merkul, S. Sergeyev, B.U.W. Maes, Potential of homogeneous Pd catalyst separation by ceramic membranes. Application to downstream and continuous flow processes, Organic Process Research & Development, 20 (2016) 911-920.

[20] I.B. Valtcheva, S.C. Kumbharkar, J.F. Kim, Y. Bhole, A.G. Livingston, Beyond polyimide: crosslinked polybenzimidazole membranes for organic solvent nanofiltration (OSN) in harsh environments, Journal of Membrane Science, 457 (2014) 62-72.

[21] P. Silva, S. Han, A.G. Livingston, Solvent transport in organic solvent nanofiltration membranes, Journal of Membrane Science, 262 (2005) 49-59.

[22] L.S. White, Development of large-scale applications in organic solvent nanofiltration and pervaporation for chemical and refining processes, Journal of Membrane Science, 286 (2006) 26-35.

[23] D. Fritsch, P. Merten, K. Heinrich, M. Lazar, M. Priske, High performance organic solvent nanofiltration membranes: Development and thorough testing of thin film composite membranes made of polymers of intrinsic microporosity (PIMs), Journal of Membrane Science, 401 (2012) 222-231.

[24] L.S. White, A.R. Nitsch, Solvent recovery from lube oil filtrates with a polyimide membrane, Journal of Membrane Science, 179 (2000) 267-274.

[25] L.S. White, Effect of operating environment on membrane performance, Current Opinion in Chemical Engineering, 28 (2020) 105-111.

[26] J.M. Hutchinson, Physical aging of polymers, Progress in Polymer Science, 20 (1995) 703-760.

[27] I.M. Hodge, Physical aging in polymer glasses, Science, (1995) 1945-1947.

[28] Z.-X. Low, P.M. Budd, N.B. McKeown, D.A. Patterson, Gas permeation properties, physical aging, and its mitigation in high free volume glassy polymers, Chemical Reviews, 118 (2018) 5871-5911.

[29] I. Sereewatthanawut, F.W. Lim, Y.S. Bhole, D. Ormerod, A. Horvath, A.T. Boam, A.G. Livingston, Demonstration of molecular purification in polar aprotic solvents by organic solvent nanofiltration, Organic Process Research & Development, 14 (2010) 600-611.

[30] X.Q. Cheng, K. Konstas, C.M. Doherty, C.D. Wood, X. Mulet, Z. Xie, D. Ng, M.R. Hill, L. Shao, C.H. Lau, Hyper-cross-linked additives that impede aging and enhance permeability in thin polyacetylene films for organic solvent nanofiltration, ACS Applied Materials & Interfaces, 9 (2017) 14401-14408.

[31] H.A. Le Phuong, C.F. Blanford, G. Szekely, Reporting the unreported: the reliability and comparability of the literature on organic solvent nanofiltration, Green Chemistry, 22 (2020) 3397-3409.

[32] S. Zeidler, U. Kätzel, P. Kreis, Systematic investigation on the influence of solutes on the separation behavior of a PDMS membrane in organic solvent nanofiltration, Journal of Membrane Science, 429 (2013) 295-303.

[33] I. Smallwood, Handbook of organic solvent properties, Butterworth-Heinemann, 2012.

[34] A.F. Barton, CRC handbook of solubility parameters and other cohesion parameters, CRC press, 1991.

[35] L.H. Sperling, Introduction to physical polymer science, John Wiley & Sons, 2005.

[36] Z. He, M. Ma, X. Lan, F. Chen, K. Wang, H. Deng, Q. Zhang, Q. Fu, Fabrication of a transparent superamphiphobic coating with improved stability, Soft Matter, 7 (2011) 6435-6443.

[37] Y.J. Chuah, Y.T. Koh, K. Lim, N.V. Menon, Y. Wu, Y. Kang, Simple surface engineering of polydimethylsiloxane with polydopamine for stabilized mesenchymal stem cell adhesion and multipotency, Scientific Reports, 5 (2015) 18162.

[38] I. Soroko, A. Livingston, Impact of TiO2 nanoparticles on morphology and performance of crosslinked polyimide organic solvent nanofiltration (OSN) membranes, Journal of Membrane Science, 343 (2009) 189-198.

[39] X. Qiao, T.-S. Chung, K. Pramoda, Fabrication and characterization of BTDA-TDI/MDI (P84) co-polyimide membranes for the pervaporation dehydration of isopropanol, Journal of Membrane Science, 264 (2005) 176-189.

[40] T. Chau, W. Bruckard, P. Koh, A. Nguyen, A review of factors that affect contact angle and implications for flotation practice, Advances in Colloid and Interface Science, 150 (2009) 106-115.

[41] M. Razali, C. Didaskalou, J.F. Kim, M. Babaei, E. Drioli, Y.M. Lee, G. Szekely, Exploring and exploiting the effect of solvent treatment in membrane separations, ACS Applied Materials & Interfaces, 9 (2017) 11279-11289.

[42] R.N. Wenzel, Resistance of solid surfaces to wetting by water, Industrial & Engineering Chemistry, 28 (1936) 988-994.

[43] J. Shen, S. Shahid, A. Sarihan, D.A. Patterson, E.A.C. Emanuelsson, Effect of polyacid dopants on the performance of polyaniline membranes in organic solvent nanofiltration, Separation and Purification Technology, 204 (2018) 336-344.

[44] C.M. Hansen, Hansen Solubility Parameters: A User's Handbook, Second Edition, CRC Press USA, 2007.

[45] E. Tarleton, J. Robinson, S. Smith, J. Na, New experimental measurements of solvent induced swelling in nanofiltration membranes, Journal of Membrane Science, 261 (2005) 129-135.

[46] T. Mohammadi, A. Aroujalian, A. Bakhshi, Pervaporation of dilute alcoholic mixtures using PDMS membrane, Chemical Engineering Science, 60 (2005) 1875-1880.

[47] J.N. Lee, C. Park, G.M. Whitesides, Solvent compatibility of poly (dimethylsiloxane)-based microfluidic devices, Analytical Chemistry, 75 (2003) 6544-6554.

[48] I. Soroko, M.P. Lopes, A. Livingston, The effect of membrane formation parameters on performance of polyimide membranes for organic solvent nanofiltration (OSN): Part A. Effect of polymer/solvent/non-solvent system choice, Journal of Membrane Science, 381 (2011) 152-162.

[49] H. Dodiuk, S.H. Goodman, Handbook of thermoset plastics, William Andrew, 2013.

[50] S. Liu, M. Chng, T. Chung, K. Goto, S. Tamai, K. Pramoda, Y. Tong, Gas‐transport properties of indan‐containing polyimides, Journal of Polymer Science Part B: Polymer Physics, 42 (2004) 2769-2779.

[51] L.S. White, Polyimide membranes for hyperfiltration recovery of aromatic solvents, in, Google Patents, 2001.

[52] S.-L. Jwo, W.-T. Whang, W.-C. Liaw, Effects of the solubility parameter of polyimides and the segment length of siloxane block on the morphology and properties of poly (imide siloxane), Journal of Applied Polymer Science, 74 (1999) 2832-2847.

[53] P. Schmidt, E.L. Bednarz, P. Lutze, A. Górak, Characterisation of organic solvent nanofiltration membranes in multi-component mixtures: Process design workflow for utilising targeted solvent modifications, Chemical Engineering Science, 115 (2014) 115-126.

[54] J. Vanneste, D. Ormerod, G. Theys, D. Van Gool, B. Van Camp, S. Darvishmanesh, B. Van der Bruggen, Towards high resolution membrane‐based pharmaceutical separations, Journal of Chemical Technology and Biotechnology, 88 (2013) 98-108.

[55] J. Robinson, E. Tarleton, C. Millington, A. Nijmeijer, Solvent flux through dense polymeric nanofiltration membranes, Journal of Membrane Science, 230 (2004) 29-37.

[56] E. Tarleton, J. Robinson, M. Salman, Solvent-induced swelling of membranes - measurements and influence in nanofiltration, Journal of Membrane Science, 280 (2006) 442-451.

[57] J. Geens, A. Hillen, B. Bettens, B. Van der Bruggen, C. Vandecasteele, Solute transport in non‐aqueous nanofiltration: effect of membrane material, Journal of Chemical Technology and Biotechnology, 80 (2005) 1371-1377.

[58] M. Bastin, K. Hendrix, I. Vankelecom, Solvent resistant nanofiltration for acetonitrile based feeds: A membrane screening, Journal of Membrane Science, 536 (2017) 176-185.

[59] P. Marchetti, A.G. Livingston, Predictive membrane transport models for Organic Solvent Nanofiltration: How complex do we need to be?, Journal of Membrane Science, 476 (2015) 530-553.

[60] P. Kisszekelyi, R. Hardian, H. Vovusha, B. Chen, X. Zeng, U. Schwingenschlögl, J. Kupai, G. Szekely, Selective electrocatalytic oxidation of biomass-derived 5-hydroxymethylfurfural to 2,5-diformylfuran: From mechanistic investigations to catalyst recovery, ChemSusChem, 13 (2020) 3127-3136.

[61] B. Scharzec, J. Holtkötter, J. Bianga, J.M. Dreimann, D. Vogt, M. Skiborowski, Conceptual study of co-product separation from catalyst-rich recycle streams in thermomorphic multiphase systems by OSN, Chemical Engineering Research and Design, 157 (2020) 65-76.

[62] P. Ahmadiannamini, X. Li, W. Goyens, N. Joseph, B. Meesschaert, I.F. Vankelecom, Multilayered polyelectrolyte complex based solvent resistant nanofiltration membranes prepared from weak polyacids, Journal of Membrane Science, 394 (2012) 98-106.

[63] G. Székely, I.B. Valtcheva, J.F. Kim, A.G. Livingston, Molecularly imprinted organic solvent nanofiltration membranes–Revealing molecular recognition and solute rejection behaviour, Reactive and Functional Polymers, 86 (2015) 215-224.

[64] S.-P. Sun, S.-Y. Chan, W. Xing, Y. Wang, T.-S. Chung, Facile synthesis of dual-layer organic solvent nanofiltration (OSN) hollow fiber membranes, ACS Sustainable Chemistry & Engineering, 3 (2015) 3019-3023.

[65] J.F. Kim, A.M.F. da Silva, I.B. Valtcheva, A.G. Livingston, When the membrane is not enough: A simplified membrane cascade using Organic Solvent Nanofiltration (OSN), Separation and Purification Technology, 116 (2013) 277-286.

[66] I.B. Valtcheva, P. Marchetti, A.G. Livingston, Crosslinked polybenzimidazole membranes for organic solvent nanofiltration (OSN): Analysis of crosslinking reaction mechanism and effects of reaction parameters, Journal of Membrane Science, 493 (2015) 568-579.

[67] R.A. R. Rautenbach, Membrane Processes, Wiley, Chichester, 1989.

[68] N. Ben Amar, H. Saidani, A. Deratani, J. Palmeri, Effect of temperature on the transport of water and neutral solutes across nanofiltration membranes, Langmuir, 23 (2007) 2937-2952.

[69] M. Tamura, T. Uragami, M. Sugihara, Synthesis and permeability of special polymer membranes: XIII. Ultrafiltration and adsorption characteristics of cellulose nitrate-activated charcoal membranes, Journal of Membrane Science, 4 (1978) 305-314.

[70] H. Saidani, N.B. Amar, J. Palmeri, A. Deratani, Interplay between the transport of solutes across nanofiltration membranes and the thermal properties of the thin active layer, Langmuir, 26 (2009) 2574-2583.

[71] R.R. Sharma, S. Chellam, Temperature effects on the morphology of porous thin film composite nanofiltration membranes, Environmental Science & Technology, 39 (2005) 5022-5030.

[72] R.E. Kesting, Synthetic polymeric membranes, McGraw Hill, New York, 1971.

[73] D.o.R. Machado, D. Hasson, R. Semiat, Effect of solvent properties on permeate flow through nanofiltration membranes. Part I: investigation of parameters affecting solvent flux, Journal of Membrane Science, 163 (1999) 93-102.

[74] R. Mahendran, R. Malaisamy, D. Mohan, Preparation, characterization and effect of annealing on performance of cellulose acetate/sulfonated polysulfone and cellulose acetate/epoxy resin blend ultrafiltration membranes, European Polymer Journal, 40 (2004) 623-633.

[75] M. Sivakumar, R. Malaisamy, C. Sajitha, D. Mohan, V. Mohan, R. Rangarajan, Ultrafiltration application of cellulose acetate–polyurethane blend membranes, European Polymer Journal, 35 (1999) 1647-1651.

[76] N. Ochoa, M. Masuelli, J. Marchese, Effect of hydrophilicity on fouling of an emulsified oil wastewater with PVDF/PMMA membranes, Journal of Membrane Science, 226 (2003) 203-211.

[77] K.M. Persson, V. Gekas, G. Trägårdh, Study of membrane compaction and its influence on ultrafiltration water permeability, Journal of Membrane Science, 100 (1995) 155-162.

[78] J. da Silva Burgal, L. Peeva, A. Livingston, Negligible ageing in poly (ether-ether-ketone) membranes widens application range for solvent processing, Journal of Membrane Science, 525 (2017) 48-56.

[79] Y.S. Toh, F. Lim, A. Livingston, Polymeric membranes for nanofiltration in polar aprotic solvents, Journal of Membrane Science, 301 (2007) 3-10.

[80] S.P. Sun, T.S. Chung, K.J. Lu, S.Y. Chan, Enhancement of flux and solvent stability of Matrimid® thin‐film composite membranes for organic solvent nanofiltration, AIChE Journal, 60 (2014) 3623-3633.

[81] H. Mariën, I.F. Vankelecom, Transformation of cross-linked polyimide UF membranes into highly permeable SRNF membranes via solvent annealing, Journal of Membrane Science, (2017).

[82] Y. Huang, D.R. Paul, Physical aging of thin glassy polymer films monitored by gas permeability, Polymer, 45 (2004) 8377-8393.

[83] M. McCaig, D.R. Paul, Effect of film thickness on the changes in gas permeability of a glassy polyarylate due to physical agingPart I. Experimental observations, Polymer, 41 (2000) 629-637.

[84] M. McCaig, D.R. Paul, J. Barlow, Effect of film thickness on the changes in gas permeability of a glassy polyarylate due to physical agingPart II. Mathematical model, Polymer, 41 (2000) 639-648.

[85] Y.H. See-Toh, F.C. Ferreira, A.G. Livingston, The influence of membrane formation parameters on the functional performance of organic solvent nanofiltration membranes, Journal of Membrane Science, 299 (2007) 236-250.

[86] I.-C. Kim, H.-G. Yun, K.-H. Lee, Preparation of asymmetric polyacrylonitrile membrane with small pore size by phase inversion and post-treatment process, Journal of Membrane Science, 199 (2002) 75-84.

[87] P. Gorgojo, S. Karan, H.C. Wong, M.F. Jimenez‐Solomon, J.T. Cabral, A.G. Livingston, Ultrathin polymer films with intrinsic microporosity: anomalous solvent permeation and high flux membranes, Advanced Functional Materials, 24 (2014) 4729-4737.